THE CFD METHODOLOGY FOR SIMULATING PUMPING LOSS FROM DISPLACER AND PISTON SEALS OF FREE PISTON STIRLING ENGINE

by

Umair MUNIR*, Asad Naeem SHAH, Muhammad Sajid KAMRAN, Muhammad FARHAN, and Zahid ANWAR

Department of Mechanical Engineering,
University of Engineering and Technology,
Lahore, Pakistan

Original scientific paper
https://doi.org/10.2298/TSCI200408295M

A new axisymmetric CFD model capable of describing pumping loss is proposed for free piston Stirling engine. Inclusion of clearance seals, bounce space, heater, cooler, and regenerator in a single model is the unique strength of this work. For transient simulation of engine, dynamic mesh was utilized for catering needs of moving boundaries. The model was validated with 12.5 kW component test power converter and successfully predicted indicated power, efficiency, pressure amplitude, pressure drop, and gas temperature in expansion and compression space at different piston amplitudes with 6% maximum deviation. The results showed that the heat exchange at heater and cooler was minimized at each flow reversal and was strongly influenced by oscillating gas-flow rate. The results also present optimum displacer and piston seal clearance at different charge pressure and operating frequencies. The displacer seal clearance could be increased up to 125 μm without compromising power, however, engine output was severely affected with increasing piston seal gap.

Key words: *Stirling engine, CFD, clearance seal, pumping loss, component test power converter*

Introduction

Depleting fossil fuels, increasing emphasis on waste heat recovery and global environment concerns of reducing emissions are some of the major factors that are driving the attention of researchers towards alternative energy conversion devices. Stirling engine is one such potential alternative candidate and has the capability to reduce reliance on fossil fuels and soothe the global warming issues. Its potential lies in its flexibility to use with any heat source, high Carnot efficiency, utilization of non-fossil fuels and operation at low temperature [1]. The Stirling engine has diverse application range from solar power generation [2], combine heat and power systems [3], and waste heat recovery systems [4] are few application area.

Modelling of Stirling engine with accuracy and completeness is a real challenge for researchers. These models are classified according to their level of complexity and accuracy [5]. Lower order models are thermodynamic models that are used in preliminary calculations. Later,

* Corresponding author, e-mail: umair.munir1@gmail.com

these models were improved by accounting irreversible losses [6] and finite time thermodynamics [7]. Although these thermodynamic models offer acceptable certainty of results, but due to their 1-D nature still lack to correctly account for the losses linked with geometric parameters. Higher order CFD models provide insight into oscillatory heat transfer and flow mechanics, which is witnessed by its use in recent studies. The developed CFD models can be categorized into 2-D axisymmetric and 3-D symmetric models.

An axisymmetric 2-D CFD model was employed for analysis of beta type Stirling engine to explain cyclic heat transfer processes [8]. To keep things simple, the fore stated model did not incorporated geometric details of heat exchangers. In another study [9] axisymmetric assumption was utilized for analysis of gamma type Stirling engine. It was reported that ensemble average temperature in the expansion space decreased at higher crank revolutions, longer displacer stroke, and for larger space between the displacer and expansion chamber wall. Alfarawi *et al.* [10] used a 2-D CFD model for gamma type Stirling engine (ST05-CNC) with tubular heater and finned cooler. An optimum phase angle of 105° was reported and engine output was improved by reducing dead volume of connecting pipe.

A 3-D CFD model was used in a recent study [11] to compare performance of a porous sheet and wire mesh regenerator by incorporating an optimization method to encompass entropy generation. The work showed lesser flow friction losses and low entropy generation with porous sheet regenerator. Xiao *et al.* [12] incorporated tubular heater and cooler in 3-D CFD model for analysis of beta type Stirling engine and compared improved simple analytical model and CFD model. Redesign of heater resulted in 1.6% improvement in overall efficiency. The complexity of flow and turbulence characteristics was studied in [13] by using multidimensional CFD method validated with ST05G engine. In [14], a discrete ordinates radiation model and displacer temperature boundary condition were used in CFD simulation further reduce the error in performance prediction of a beta type Stirling engine prototype.

In past, CFD approach has been frequently used by researchers to investigate alpha, beta, and gamma variants of Stirling engine due to simplified geometry and predefined piston motions. But, there is limited work to develop a CFD code for free piston Stirling engine (FPSE), this is due to its abrupt piston and displacer motion and geometric complexities. The motion of piston and displacer is considered nearly sinusoidal at steady-state operation as reported by Lewandowski *et al.* [15] for component test power converter (CTPC). The pumping loss data from displacer and piston clearance seals is also not commonly available. Therefore, this work aims to develop a new axisymmetric CFD model for 12.5 kW CTPC, which can predict indicated power, efficiency, and pumping losses under oscillatory flow conditions. In the start focus in on analysis of cyclic thermal and flow fields whereas later portion presents details on effect of displacer and piston clearance size on periodic gas leakage and power output.

Description of engine geometry and operating conditions

The CTPC developed by NASA [16] for space power application has been used in this study for validation. The schematic diagram of CTPC is shown in fig. 1. The engine was equipped with a star fish heater maintained at 800 K and a cross-flow internally finned tube cooler maintained at 400 K. A screen matrix regenerator with 72.8% porosity and 3.76 cm length was placed between heater and cooler as heat reservoir. The gas was oscillated between hot space and cold space due to motion of displacer and power pistons with 70.83° phase difference. The engine used helium as working gas with 15 MPa charge pressure. Some of important engine input parameters that were used in development of computational domain are given in tab. 1.

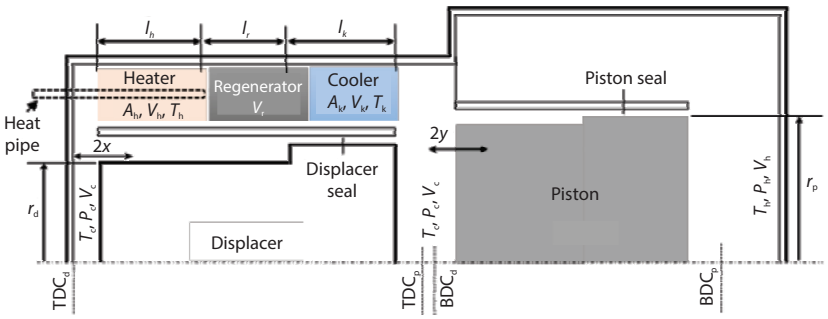

Figure 1. Schematic of CTPC

Table 1. Input parameters of CTPC

Parameter	Value	Parameter	Value
Displacer radius, r_d [mm]	57.15	Cooler (internal finned tube)	
Piston radius, r_p [mm]	68.5	Fin (channel) height [mm]	1.464
Displacer amplitude, X [mm]	14.8	Fin (channel) width [mm]	0.533
Piston amplitude, Y [mm]	13.44	Fin (channel) total length [mm]	74.93
Expansion space mean volume, V_{eo} [m^3]	$4.28\cdot10^{-4}$	Fin (channel) active length [mm]	64.77
Compression space mean volume, V_{co} [m^3]	$6.35\cdot10^{-4}$	Active heat transfer area for cooler, A_k [m^2]	0.667
Heater (annular starfish finned)		Cooler dead volume, V_k [m^3]	1.74×10^{-4}
Diameter of heater channel [mm]	1.016	Clearance seals	
Total number of channels	1900	Displacer seal clearance, δ_d [mm]	0.076
Total heater channel length, l_h [mm]	59.7	Displacer seal length [mm]	50.8
Active heater channel length	54.6	Piston seal clearance, δ_p [mm]	0.016
Active heat transfer area for heater, A_h [m^2]	0.3317	Piston seal length [mm]	51.8
Heater dead volume, V_h [m^3]	$1.14\cdot10^{-4}$	Appendix gap clearance [mm]	0.311
Regenerator (annular screen matrix)		Operating conditions	
Outside diameter of matrix [mm]	227.8	Working fluid	He
Inside diameter of matrix [mm]	116.9	Charge pressure, P [MPa]	15
Wire diameter, d_w [mm]	0.0508	Heater wall temperature, T_h [K]	800
Regenerator length, l_r [mm]	37.6	Cooler wall temperature, T_k [K]	400
Regenerator porosity, β [%]	72.8	Operating frequency, f [Hz]	67.45
Regenerator dead volume, V_r [m^3]	$8.22\cdot10^{-4}$	Phase angle, ϕ [°]	70.83

The CFD model

The flow inside the engine was oscillatory and considered as unsteady, compressible and turbulent. This complex flow and heat transfer phenomenon was solved by using commercially available CFD package ANSYS FLUENTl 15.0.

Governing equations

The governing equations of mass, momentum, and energy that were solved to calculate spatial and time variation of velocity, temperature, and pressure were written in the form of cylindrical co-ordinates.

The conservation of mass is given:

$$\frac{\partial \rho}{\partial t}+\frac{\partial}{\partial x}(\rho u)+\frac{1}{r}\frac{\partial}{\partial r}(\rho r v)=0 \tag{1}$$

where x is the axial co-ordinate, r – the radial co-ordinate, ρ – the density of working fluid, u – the axial velocity, and v – the radial velocity. The conservation of momentum in axial and radial direction is given:

$$\frac{\partial}{\partial t}(\rho u)+\frac{1}{r}\frac{\partial}{\partial x}(r\rho uu)+\frac{1}{r}\frac{\partial}{\partial r}(r\rho vu)=\rho g-\frac{\partial p}{\partial x}+$$
$$+\frac{1}{r}\frac{\partial}{\partial x}\left\{r\mu\left[\frac{2\partial u}{\partial x}-\frac{2}{3}(\nabla\vec{v})\right]\right\}+\frac{1}{r}\frac{\partial}{\partial r}\left[r\mu\left(\frac{\partial u}{\partial r}+\frac{\partial v}{\partial x}\right)\right] \tag{2}$$

$$\frac{\partial}{\partial t}(\rho v)+\frac{1}{r}\frac{\partial}{\partial x}(r\rho uv)+\frac{1}{r}\frac{\partial}{\partial r}(r\rho vv)=-\frac{\partial p}{\partial r}+\frac{1}{r}\frac{\partial}{\partial x}\left[r\mu\left(\frac{\partial v}{\partial x}+\frac{\partial u}{\partial r}\right)\right]+$$
$$+\frac{1}{r}\frac{\partial}{\partial r}\left\{r\mu\left[2\frac{\partial v}{\partial r}-\frac{2}{3}(\nabla\vec{v})\right]\right\}-2\mu\frac{v}{r^2}+\frac{2}{3}\frac{\mu}{r}(\nabla\vec{v})+\rho\frac{v^2}{r}+F_r \tag{3}$$

The conservation of energy is given:

$$\frac{\partial}{\partial t}(\rho T)+\frac{\partial}{\partial x}(\rho uT)+\frac{1}{r}\frac{\partial}{\partial r}(r\rho vT)=$$
$$=-\frac{1}{c_p}\left[\frac{\partial p}{\partial r}+\nabla(pV)-p(\nabla V)\right]+\frac{k}{c_p}\left[\frac{\partial}{\partial x}\left(\frac{\partial T}{\partial x}\right)+\frac{1}{r}\frac{\partial}{\partial r}\left(r\frac{\partial T}{\partial r}\right)\right]+$$
$$+\frac{\mu}{c_p}\left\{2\left[\left(\frac{\partial u}{\partial x}\right)^2+\left(\frac{\partial v}{\partial x}\right)^2+\left(\frac{v}{r}\right)^2\right]+\left[\left(\frac{\partial v}{\partial x}+\frac{\partial u}{\partial r}\right)^2-\frac{2}{3}(\nabla V)^2\right]\right\} \tag{4}$$

where T is the temperature, k – the thermal conductivity, and c_p – the specific heat of gas.

Porous media model (regenerator)

Regenerator was modeled by using porous media sub-model available in ANSYS FLUENT. Pressure drop along the regenerator length was estimated with Darcy-Forcheimer equation. Input parameters for modelling a regenerator as porous media were permeability, inertial coefficient and porosity, which were evaluated by the data provided in [16]. Pressure drop along the regenerator length is given:

$$\frac{\nabla p}{L}=\frac{\mu}{K}u+\frac{C_f}{\sqrt{K}}\rho u^2 \tag{5}$$

where K is the permeability and C_f – the inertial resistance coefficient given, respectively:

$$K=\frac{2d_{\mathrm{h}}^2}{\alpha} \tag{6}$$

$$C_f=\frac{\delta R_{\mathrm{e}}^{\gamma}}{\sqrt{2\alpha}} \tag{7}$$

where d_h is the hydraulic diameter and $\alpha = 129$, $\delta = 2.91$, and $\gamma = -0.103$ are constant for woven wire screens [17].

Computational domain and meshing

The geometric and operating parameters of CTPC given in tab. 1 were used to build the computational domain. Initially, displacer was set at its mid stroke position, whereas piston was set near its BDC having 70.83° phase difference as shown in fig. 2. Expansion and compression spaces were modeled on the basis of displacer radius (57.15 mm) and piston radius (68.5 mm) and their respective stroke amplitudes. Heater in 2-D was modeled by matching hydraulic diameter, passage length, gas volume, and heat transfer area. Six narrow channels were built having 0.508 mm gap as hydraulic radius, 0.318 m^2 heat transfer area, $1.09 \cdot 10^{-4}$ m^3 gas volume, and 54.6 mm active heat transfer length. Similarly, cooler was matched in 2-D by creating ten narrow channels having 0.39 mm gap as hydraulic radius, 0.657 m^2 heat transfer area, $1.68 \cdot 10^{-4}$ m^3 gas volume, and 64.77 mm active heat transfer length.

In meshing, computation domain was divided into eight zones and each zone was separately meshed. Expansion and compression spaces were meshed using mapped face meshing having quadrilateral cells of 0.6 mm size. Refined mesh was used at the heater and cooler boundary walls for accurate boundary-layer formation and heat transfer. The mesh was refined by using edge sizing and bias factor features. Narrow channels like appendix gap, displacer and piston seals were also meshed by using mapped face meshing, edge sizing and bias factor tools. The regenerator zone was meshed by using the face sizing tool having cell size of 0.3 mm. The computational domain used in this study was made of 96508 elements having average orthogonal quality of 0.97 and average skewness of 0.07.

Boundary conditions, solution procedure, and mesh independence

The boundary conditions were carefully assigned as this is a crucial step to obtain accurate and validated results. Heater and cooler walls were set as isothermal with wall temperatures of 800K and 400K, respectively. Exterior engine walls, moving displacer and piston walls were considered as adiabatic. The motion of piston and displacer was defined by a user defined function. A transient, pressure based axisymmetric solver with standard k-ε turbulence sub model was used to solve the governing equations.

In grid independence study, the sensitivity of results was examined by coarse, medium and fine mesh having 74649, 96508, and 162048 cells, respectively. The variation in power output by using medium and fine mesh was 1.5%. Further refinement of mesh resulted in significantly high computational cost. Therefore, medium mesh with 96508 cells was selected in this study. Selection of time step size is another critical task. Therefore, 360 and 180 time

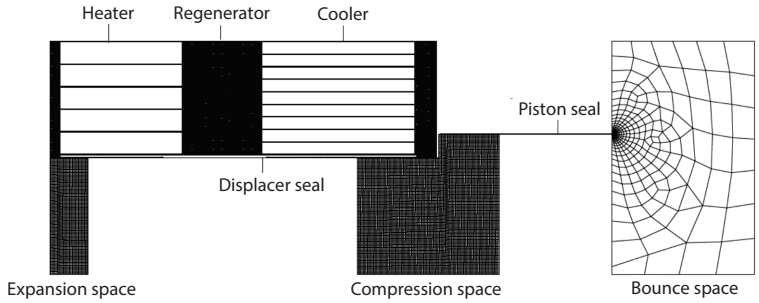

Figure 2. Computational domain of CTPC

steps/cycle were compared and it was found that 360 time steps/cycle showed better convergence and accuracy of results up to 98%.

Model validation

The developed axisymmetric model was successfully tested to reproduce the experimental results summarized in [16]. In fig. 3(a), Indicated power obtained from simulation was compared with experiment at default operating conditions. The comparison indicated that power was predicted with maximum 6% deviation. The shuttle heat loss associated with gas entrapped in displacer was neglected, however, the observed deviation is lying with in experimental uncertainty and thus confirms validation of numerical approach. The comparison was further extended and close agreement was noticed in the prediction of indicated efficiency as shown in fig. 3(b). In figs. 3(c) and 3(d), pressure drop across the heater, regenerator and cooler circuit and amplitude of pressure wave are plotted at different piston amplitudes for further validation of current model. The amplitude of pressure wave was slightly over predicted, however, pressure drop was under estimated. The effect of piston amplitude on expansion space and compression space gas temperature was evaluated and plotted in figs. 3(e) and 3(f). It can be seen that results were in close agreement to experiment and 2-D analogy of heat exchangers worked well.

Results and discussion

Cyclic thermal and flow fields

This section explains cyclic variation of temperature, pressure and heat transfer rate after reaching steady-state. The flow of working gas inside FPSE was completely reversing in one cycle and its direction was reversed through heater and cooler channels twice. In fig. 4(a), cyclic variation of gas temperature in expansion space and heat transfer rate at heater wall are presented. It can be observed that expansion space temperature reached its maximum (772 K) at 176° CA at the end of compression process. Heat transfer rate at heater wall was dipped twice during a cycle due to reduced mass-flow rate of gas at each flow reversal. In fig. 4(b), temperature variation of compression space and heat rejected at cooler are presented. Evidently, the amount of heat rejected in cooler was minimized during 260°-290° CA, which was due to reduced mass-flow rate of gas in cooler channels during flow reversal.

Contours of static pressure and streamlines are shown in fig. 5 at four CA. It can be observed that pressure inside different engine spaces was not uniform due to flow losses across engine auxiliaries. The major pressure loss as expected was across regenerator. The working gas was moving to compression space in the beginning of the cycle as illustrated by streamlines in fig. 5(a). A tumble vortex formed in the compression space due to turbulent jetting of gas from cooler channels and displacer seal. The flow direction of gas was reversed at 90° when displacer was passing its TDC as shown in fig. 5(b). Turbulence was observed in flow jets exiting heater channels form smaller swirls before its entry to the expansion space. Compression of gas continued during 339°-159° and maximum pressure was observed in compression space at 172° as indicated in fig. 5(c). However, expansion of gas started at 160° and continued until 338° CA and minimum pressure was observed in the compression space during the expansion process. The flow direction was reversed again at 260° in the middle of expansion process as shown in fig. 5(d). The vortices formed inside hot space and cold space lost its intensity close to the wall and diminishes at the wall because of no slip condition.

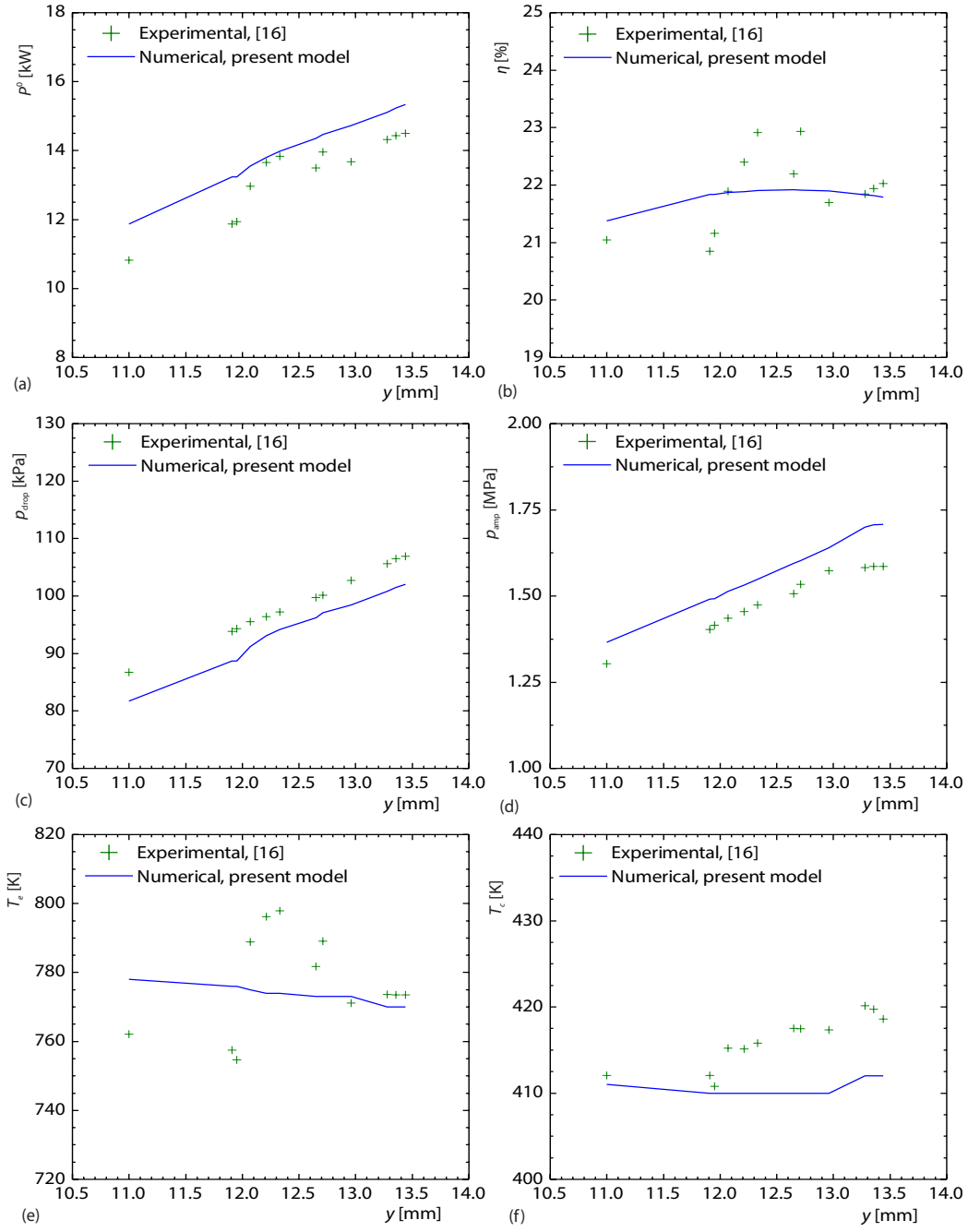

Figure 3. Comparison of experimental [16] and simulation results; (a) indicated power, (b) indicated efficiency, (c) pressure drop, (d) pressure amplitude, (e) expansion space temperature, and (f) compression space temperature *vs.* piston amplitude

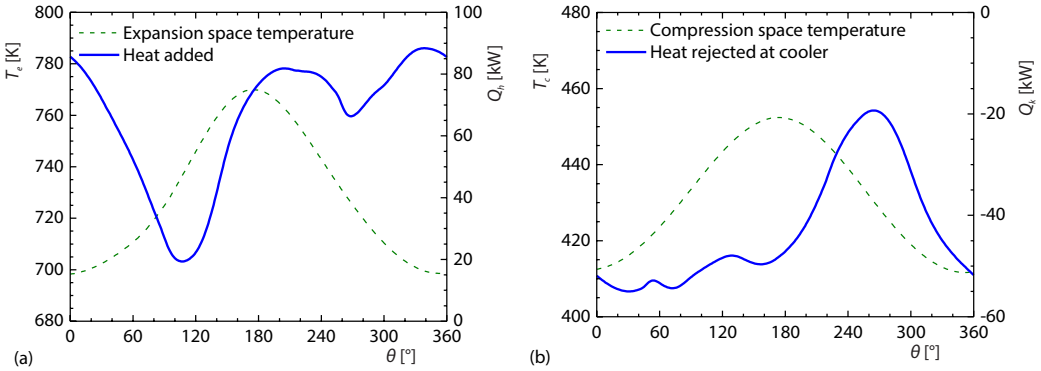

Figure 4. Instantaneous temperature and heat transfer rate at (a) expansion space and heater and (b) compression space and cooler

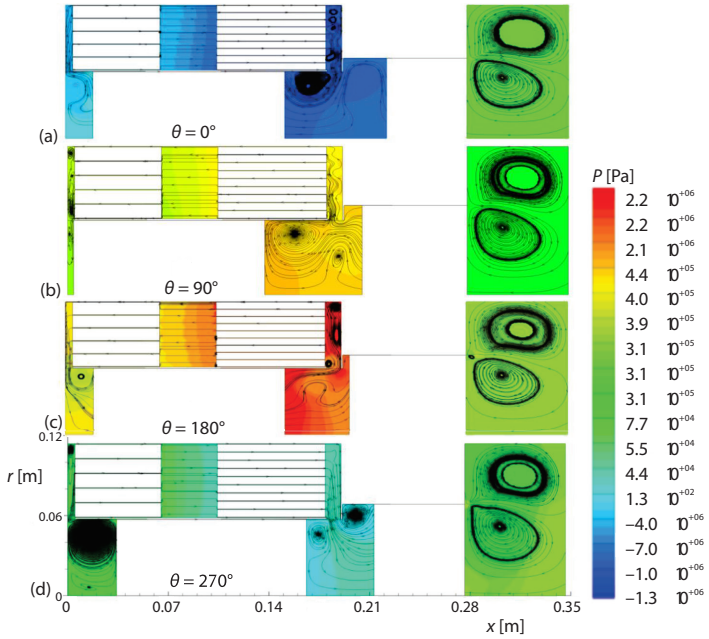

Figure 5. Pressure contour and streamlines at four different CA during 30th cycle

Effect of displacer and piston clearance seal

In this section, effect of displacer and piston clearance seal is described for maximum power at different operating frequencies and charge pressures. Since, tight radial clearance between piston and cylinder provides a secondary high resistance passage for gas-flow. The leakage of working gas from these tight clearances is termed as pumping loss. Displacer seal was represented by a narrow bypass passage having 76 μm radial clearance and 50.8 mm seal length. Another narrow passage was made between compression space and bounce space having 16 μm radial clearance and 51.8 mm seal length to represent piston seal.

Leakage of working gas from displacer and piston seal is shown in fig. 6. The displacer seal leakage was obtained at the opening end of seal in cold compression space, whereas piston seal leakage was computed at the seal end that was opening in bounce space. Evidently, gas-flow from both of the seals was periodic and completely reversing in one cycle. It was observed that pumping loss from displacer seal was a function of pressure difference between expansion space and compression space. Similarly, pumping loss from piston seal was influenced by pressure difference between compression space and bounce space during one cycle.

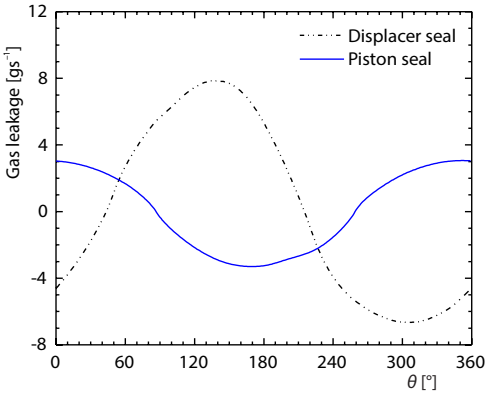

Figure 6. Periodic gas leakage from displacer and piston seals

The effect of displacer seal clearance on CTPC power and gas leakage at different charge pressures is presented in fig. 7(a). The gas leakage from displacer seal was averaged for both hot blow and cold blow during the cycle and then plotted. It was observed that power remained almost unaffected at displacer clearance between 76-125 μm. However, it decreased sharply as clearances increases from 125 μm. The effect of displacer seal clearance was further investigated at three different frequencies (60 Hz, 67.45 Hz, and 80 Hz) and results are

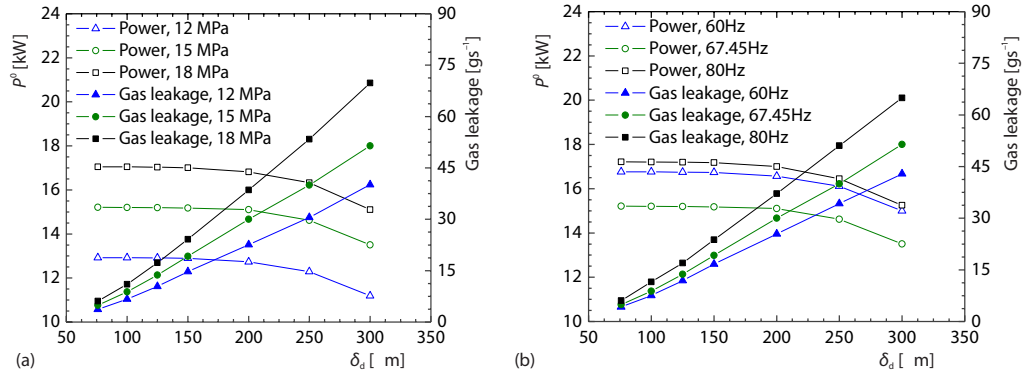

Figure 7. Effect of displacer seal clearance on power and gas leakage at (a) 67.45 Hz and (b) 15.0 MPa

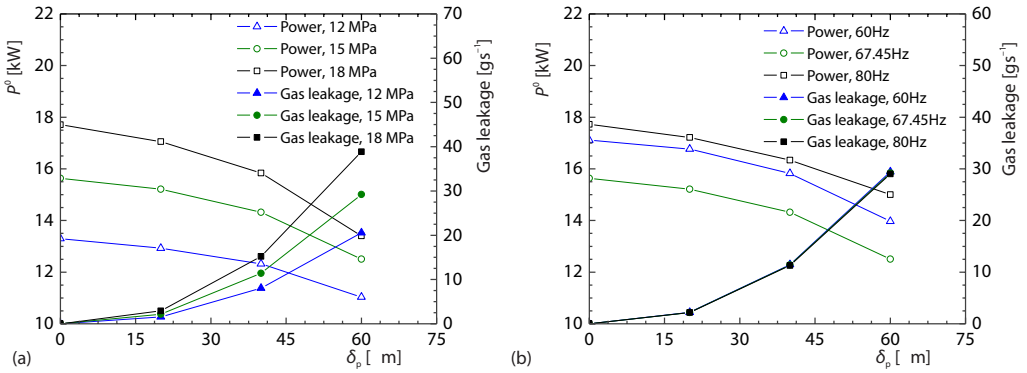

Figure 8. Effect of piston seal clearance on power and gas leakage at (a) 67.45 Hz and (b) 15.0 MPa

compared in fig. 7(b). Evidently, the gas leakage through displacer seal was increasing with clearance size as well as with operating frequency. It was observed that pumping loss increased significantly as displacer clearance crosses 125 μm limit. Therefore, the design of displacer clearance seal could be improved by adjusting to higher clearance. Displacer clearance could be increased up to 125 μm, which may decrease frictional losses and avoid machining difficulties.

In fig. 8(a), the effect of piston seal clearance on engine power and gas leakage is presented at different charge pressures (12 MPa, 15 MPa, and 18MPa). Evidently, maximum power was obtained at zero piston seal clearance, which was computed without incorporating the piston seal and bounce space in the model. However, zero piston seal clearance is not possible practically. It was also observed that the effect of charge pressure on pumping loss was intensified on higher piston seal clearances. Piston seal clearance effect was also examined at three different frequencies (60 Hz, 67.45 Hz, and 80 Hz) and results were compared in fig. 8(b). It can be seen that pumping loss from piston seal was only affected by clearance gap and effect of operating frequency was marginal.

Conclusions

In this work an axisymmetric CFD models was developed for FPSE, the model was validated with CTPC to examine cyclic thermal and flow fields and effect of displacer and piston seals. Some of the key findings are presented as follows.

- The maximum deviation between simulation and experiment was less than 6% for prediction of power, efficiency, gas temperatures, and flow losses.
- The heat transfer rate at heater and cooler was strongly affected by oscillatory gas-flow rate and minimized at every flow reversal. Also, temperature of gas in hot and cold sides were function of time and space.
- The pumping loss from displacer seal became significant as clearances increases beyond 125 μm. Therefore, the actual displacer design could be modified by increasing clearance from 76 μm.
- The CTPC output was observed to be severely affected by increasing piston seal clearance.

Acknowledgment

The authors would like to acknowledge the University of Engineering and Technology, Lahore for sponsoring this research work under grant number ORIC/103-ASRB/3404.

Nomenclature

A – area, [m^2]
C_f – friction coefficient
d_h – hydraulic diameter, [m]
d_w – regenerator wire diameter, [m]
K – permeability, [m^2]
l – length, [mm]
P^0 – indicated power, [kW]
P – mean pressure, [MPa]
Q – heat transfer rate, [kW]
r – radius, [mm]
T – temperature, [K]
V – volume, [m^3]
X – displacer amplitude, [m]
Y – piston amplitude, [m]

Greek symbols

δ – seal clearance, [μm]
θ – crank angle, [°]
μ – viscosity, [m^{2}s–1]

Subscript

co – compression space
eo – expansion space
d – displacer
h – heater
k – cooler
p – piston
r – regenerator

References

[1] Wang, K., *et al.*, Stirling Cycle Engines for Recovering Low and Moderate Temperature Heat: A Review, *Renewable and Sustainable Energy Reviews*, *62* (2016), Suppl. C, pp. C89-C108
[2] Shendage, D. J., *et al*., Numerical Investigations on the Dish-Stirling Engine System, *International Journal of Ambient Energy*, *40* (2019), 3, pp. 274-284
[3] Ribberink, H., *et al*., A Plausible Forecast of the Energy and Emissions Performance of Mature-Technology Stirling Engine Residential Cogeneration Systems in Canada, *Journal of Building Performance Simulation*, *2* (2009), 1, pp. 47-61
[4] Bani-Hani, E., *et al.*, Enhancing Cooling System of a Combustion Engine by Integrating with a Stirling Cycle, *Energy Engineering*, *116* (2019), 3, pp. 41-53
[5] Ahmadi, M. H., *et al*., Thermal Models for Analysis of Performance of Stirling Engine: *A Review*, *Renewable and Sustainable Energy Reviews*, *68* (2017), Part 1, pp. 168-184
[6] Ye, W., *et al*., Exergy Loss Analysis of the Regenerator in a Solar Stirling Engine, *Thermal Science*, *22* (2018), Suppl. 2, pp. S729-S737
[7] Sharma, A., *et al*., Finite Time Thermodynamic Analysis and Optimization of Solar-Dish Stirling Heat Engine with Regenerative Losses, *Thermal Science*, *15* (2011), 4, pp. 995-1009
[8] Salazar, J. L.,Chen, W.-L., A Computational Fluid Dynamics Study on the Heat Transfer Characteristics of the Working Cycle of a *β*-Type Stirling Engine, *Energy Conversion and Management*, *88* (2014), Suppl. C, pp. C177-C188
[9] Kato, Y., *et al*., Effect of Geometry and Speed on the Temperatures Estimated by CFD for an Isothermal Model of a Gamma Configuration Low Temperature Differential Stirling Engine with Flat-Shaped Heat Exchangers, *Applied Thermal Engineering*, *115* (2017), Suppl. C, pp. C111-C122
[10] Alfarawi, S., *et a*l., Influence of Phase Angle and Dead Volume on Gamma-Type Stirling Engine Power Using CFD Simulation, *Energy Conversion and Management*, *124* (2016), Suppl. C, pp. C130-C140
[11] Li, Z., *et al.*, Analysis of a High Performance Model Stirling Engine with Compact Porous-Sheets Heat Exchangers, *Energy*, *64* (2014), C, pp. 31-43
[12] Xiao, G., *et al*., Design Optimization with Computational Fluid Dynamic Analysis of *β*-Type Stirling Engine, *Applied Thermal Engineering*, *113* (2017), Suppl. C, pp. C87-C102
[13] Kuban, L., *et al.*, A 3D-CFD Study of a *γ*-Type Stirling Engine, *Energy*, *169* (2019), Feb., pp. 142-159
[14] Caetano, B. C., *et al*., A Novel Methodology on Beta-Type Stirling Engine Simulation Using CFD, *Energy Conversion and Management*, *184* (2019), Mar., pp. 510-520
[15] Lewandowski, E. J., Johnson, P. K., Stirling System Modelling for Space Nuclear Power Systems, *Proceedings*, Space Nuclear Conference, Boston, Mass. USA, 2007
[16] Dhar, M., Stirling Space Engine Program, Final Report, NASA, 1999, Vol. 1
[17] Tew, R., *et al*. An Initial Non-Equilibrium Porous-Media Model for CFD Simulation of Stirling Regenerators, *Proceedings*, 4th International Energy Conversion Engineering Conference and Exhibit (IECEC), San Diego, Cal., USA, 2006, p. 4003

Paper submitted: April 8, 2020
Paper revised: June 8, 2020
Paper accepted: September 1, 2020